Journal of Magnetism and Magnetic Materials 489 (2019) 165447

Contents lists available at ScienceDirect

Journal of Magnetism and Magnetic Materials

journal homepage: www.elsevier.com/locate/jmmm

Research articles

Collective modes of three-dimensional magnetic structures: A study of target skyrmions

Alexander C. Booth[a], Yizhou Liu[b,c,*], Jiadong Zang[a]

[a] Department of Physics and Astronomy, University of New Hampshire, Durham, NH 03824, USA
[b] Beijing National Laboratory for Condensed Matter Physics, Institute of Physics, Chinese Academy of Sciences, Beijing 100190, China
[c] Department of Electrical and Computer Engineering, University of California, Riverside, CA 92507, USA

ARTICLE INFO

Keywords:
Skyrmion
Magnetic resonance

ABSTRACT

Three-dimensional magnetic textures present their richness not only in variety of ground state structures, but also in their dazzling collective modes. As an example, the target skyrmion, a topological spin texture with a central skyrmion and an extra concentric helical ring, has been enabled by confining a chiral magnet in a nanodisk geometry. In this work we investigate the collective spin wave modes of the target skyrmion in the external field region of −400 mT to 400 mT. Through micromagnetic simulations we reproduced three major phases of the target skyrmion, and derived resonance modes at varying external magnetic field by the power spectral density study. All typical modes were resolved in terms of their dynamical snapshots in temporal domain and the corresponding spatial Fourier transformations. Some modes are shown to behave similarly in-plane but differently out-of-plane, and vice versa. This suggests, on a broader scope, that both responses will be necessary to fully characterize collective modes of three-dimensional spin textures.

1. Introduction

Nanoscale magnetic systems can host diverse magnetic structures with different dimensionalities. They are not only of fundamental interests but also promising for many potential applications [1,2]. While low-dimensional magnetic structures, such as domain walls and skyrmions, have been extensively studied [3,4], their three-dimensional (3D) counterparts have not yet been fully exploited. Recent works, including theoretical predictions and experimental observations of 3D magnetic structures [5–8], have greatly extended the scope of 3D magnetic structures. The complicated spin configurations of 3D magnetic structures may lead to exotic physics and novel device applications [9]. Thus, it is of vital importance to understand their static and dynamic properties.

Magnetic skyrmions are topologically protected, particle-like spin textures. They can be stabilized in thin films or bulk crystals with the Dzyaloshinkii-Moriya (DM) interaction [10,11] induced by the breaking of inversion symmetry. Although usually regarded as a two-dimensional (2D) spin texture, the skyrmion also plays an active role in constituting 3D magnetic structures, e.g., simple stacking of skyrmions can form skyrmion tubes [12], and skyrmions in combination with Bloch points can form the so-called chiral bobbers [8]. The formation of these 3D magnetic configurations originated from the competition between different magnetic interactions (such as the exchange interaction and the DM interaction) and their stabilities can be further enhanced by geometrical confinements [13–16]. A good example is the recently observed target skyrmion in FeGe nanodisk [17,21,22], i.e., a central skyrmion with surrounding concentric helical ring(s) near the edge of the disk. The target skyrmion is stable even in the absence of external magnetic field, which is an attractive property for practical applications. Furthermore, due to the addition of a third spatial dimension in its magnetic configuration, it becomes one of few examples of 3D magnetic structure for dynamical resonance study.

Here, we theoretically study the dynamics of a target skyrmion in detail. Phase diagram of the resonant band is explored under varying external magnetic field applied along the disk axis. The ground state configurations of a target skyrmion under a static external field that extends from −400 mT to 400 mT are first obtained using micromagnetic simulations. It is noted that, depending on the skyrmion polarity and the field direction, the target skyrmion undergoes a transition from π skyrmion to 2π skyrmion [23] at small fields and can even switch its polarity at large fields. We then calculate the power spectrum of the out-of-plane resonant modes and examine its evolution as a function of the static external field. Individual resonance modes are resolved using dynamical simulations and their modulations along azimuthal, radial and vertical directions are analyzed and discussed

* Corresponding author at: Beijing National Laboratory for Condensed Matter Physics, Institute of Physics, Chinese Academy of Sciences, Beijing 100190, China.
E-mail address: yliu062@ucr.edu (Y. Liu).

https://doi.org/10.1016/j.jmmm.2019.165447
Received 25 February 2019; Received in revised form 13 May 2019; Accepted 11 June 2019
Available online 12 June 2019
0304-8853/ © 2019 Elsevier B.V. All rights reserved.

[24,25].

2. Methodology

In the continuum approximation, the Hamiltonian density of a chiral magnet can be written as

$$\mathscr{H} = -A(\nabla \mathbf{S})^2 - D\mathbf{S}\cdot(\nabla \times \mathbf{S}) - \mu_0 M_s \mathbf{H}\cdot\mathbf{S} + \mathscr{H}_{dip} \quad (1)$$

where $\mathbf{S}$ represents the unit vector of magnetization, A is the exchange constant, D is the strength of the DM interaction, M_s is the saturation magnetization and the last two terms are the Zeeman and dipole-dipole interactions, respectively. This anisotropy-free Hamiltonian well captures the phase diagram of target skyrmions, as reported in Ref. [22].

Using this model, the ground state of target skyrmion and the corresponding dynamic response to an a.c. magnetic field were computed using the open source micromagnetic simulation software package *mumax*^{3}[26]. *mumax*^{3} numerically integrates the Landau-Lifshitz-Gilbert (LLG) equation [27,28]

$$\dot{\mathbf{S}} = -|\gamma_0|\mathbf{S} \times \mathbf{H}_{\mathbf{eff}} + \alpha \mathbf{S} \times \dot{\mathbf{S}} \quad (2)$$

where γ_0 is the gyromagnetic constant, α is the Gilbert damping constant and $\mathbf{H}_{\mathbf{eff}} = -\frac{1}{\mu_0 M_s}\frac{\delta \mathscr{H}}{\delta \mathbf{S}}$ is the effective field. For the simulations performed in this work, the exchange constant $A = 8.78$ pJ/m, DM interaction strength of $D = 1.58$ mJ/m^2, saturation magnetization $M_s = 384$ kA/m and damping constant $\alpha = 0.001$ are employed. The geometry of the nanodisk is diameter $d = 160$ nm with height $h = 90$ nm and the meshed cell size is 4 nm × 4 nm × 3 nm. Smaller cell size (2 nm × 2 nm × 1.5 nm) is also used to confirm the simulations and the final results reported here are independent of mesh size choices.

The simulations considered here are comprised of both ground state relaxations and dynamic simulations. First, the ground state of the target skyrmion is determined in the presence of a static, perpendicular applied external magnetic field along the z axis. An initial skyrmion state is created in the center of the nanodisk and the energy is then minimized in order to get the ground state. Then the skyrmion dynamics are computed about this ground state by including an additional a.c. external magnetic field in the z direction, described by the cardinal sine function $H_{ac}\frac{\sin 2\pi\omega_c t}{2\pi\omega_c t}$, where $\omega_c = 25$ GHz is the cutoff frequency up to which collective modes will be excited and the amplitude $H_{ac} = 5$ mT. The simulation is then run for a period of 20 ns, with data sampled every 5 ps.

3. Ground state configurations

Ground states of target skyrmions under different static external magnetic fields are discussed in this section. A static external magnetic field is applied along z direction in intervals of 10 mT from − 400 mT to 400 mT. It has been reported that two types of target skyrmions with opposite polarity can be hosted in chiral magnet nanodisk. Without loss of generality, a skyrmion with polarity $p = -1$ is employed here as the initial state at zero field, where the sign of p is determined by the magnetization direction at the core of skyrmion. $p = +1$ target skyrmion's evolution as a function of the external field can be readily mapped out by reversing all magnetizations.

Fig. 1 shows the top-down view of four sample spin configurations obtained. The resulting spin textures are target skyrmions with varying numbers of concentric helical rings. A $p = -1$ target skyrmion is stabilized at 0 mT (Fig. 1c). When applying an external magnetic field in $+z$ direction, the central skyrmion shrinks as the field increases and there is no obvious change of the spin texture until reaching the maximum field value. When an external magnetic field along $-z$ direction is applied, the central skyrmion transforms from a π skyrmion to a 2π skyrmion at − 120 mT. Further increasing the field to − 280 mT results in a switching of the target skyrmion polarity from $p = -1$ to $p = 1$. Fig. 1(a) has a central skyrmion with an additional edge twist around the outside and is symmetrical with opposite helicity and polarity to the same texture at 350 mT. Fig. 1(b) is a 2π skyrmion with an edge twist and (c) is a π skyrmion. All the collective modes calculations in the following sections are based on the ground states discussed above.

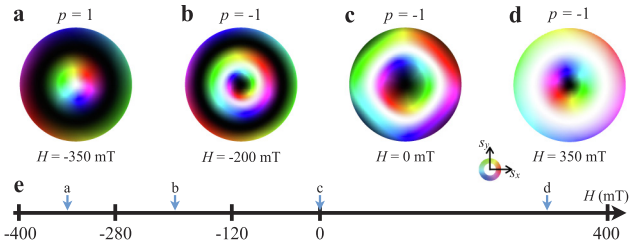


Fig. 1. Evolution of target skyrmion as a function of external magnetic field. a–d Top surface of static target skyrmion configurations for different external field values: a − 350 mT, b − 200 mT, c 0 mT and d 350 mT. Color represents the in-plane angle and black (white) represents negative (positive) z direction. e. Phase diagram of the target skyrmion. (For interpretation of the references to colour in this figure legend, the reader is referred to the web version of this article.)

4. Spin wave modes of target skyrmions

4.1. Determining the modes

The power spectral density (PSD) for each dynamical simulation was calculated by taking the Fourier transformation of the fluctuations in the spatially averaged z component of the magnetization $\delta S_z(t) = \langle S_z(t)\rangle - \langle S_{z,0}\rangle$. This was done for each value of the external field from − 400 mT to 400 mT in increments of 10 mT and the collective result is shown in Fig. 2. There are two discontinuities in the PSD map, which are corresponding to the transformation from a π skyrmion to a 2π skyrmion at − 120 mT and the switching of the target skyrmion polarity at − 280 mT, respectively.

At zero magnetic field, twelve significant modes are identified in the PSD map. The frequencies of these modes show non-monotonic behaviors as a function of the applied magnetic field. For positive applied fields, these twelve modes finally merge into three significant modes and the frequencies of these three modes monotonically decrease with increasing field until reaching 400 mT. In contrast, at negative applied fields, these twelve modes merge into three significant modes around

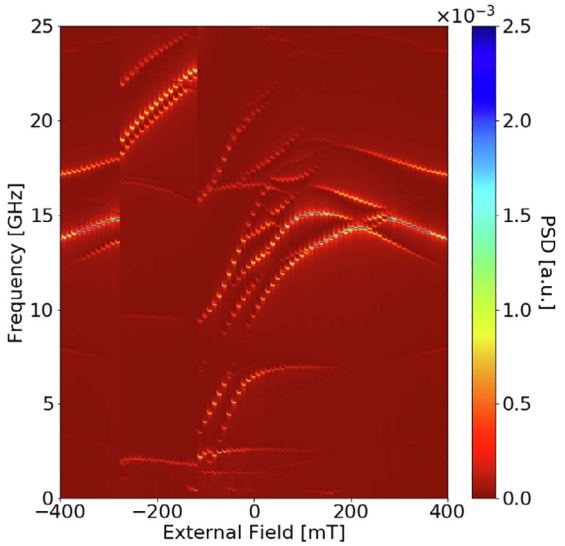


Fig. 2. Spectrum of the target skyrmion response as funtion of the external static magnetic field.

− 120 mT, the transition point from a π skyrmion to a 2π skyrmion. In addition to the three merged modes, three new significant modes emerge in the spectrum. This might be explained by the formation of an additional helical ring and the 2π skyrmion. Further increasing the field to − 280 mT results in the switching of skyrmion polarity and a discontinuity is observed in the PSD map. The corresponding collective modes in this regime are symmetrical with the three significant modes in the positive field regime with the same amplitude since the target skyrmion textures in these two regimes are also symmetric with each other. A subsequent spatial Fourier transformation is then performed on each dynamical simulation and detailed analysis of the collective modes will be discussed below.

4.2. Spatially resolved collective modes

To further understand the collective modes in details, each mode was resolved by starting with a relaxed target skyrmion at a particular static external magnetic field and driving it with an a.c. magnetic field, $H_{ac}\sin 2\pi\omega t$ where $H_{ac} = 5$ mT is the amplitude and ω is the frequency in consideration. The resulting real time dynamics of the fluctuations in the z component of the magnetization and the corresponding spatial Fourier transformations were then investigated. We confirmed that the dynamical patterns on the same band in Fig. 2 share similar features, so that we only need to investigate one typical point on each band only. Since a target skyrmion is composed of a central skyrmion with surrounding concentric helical ring(s), its collective modes should develop some patterns in both the radial and azimuthal directions, similar to that of the collective modes of a simple skyrmion. Some nodes will be developed, at which the spin deviation δS_z vanishes. In addition, the finite thickness of target skyrmion is not negligible and it may lead to some collective modes along the vertical (disk normal) direction. Thus, it is necessary to characterize each mode of target skyrmion in terms of the number of nodes in: radial N_r, azimuthal N_a and vertical N_v directions. We mainly focus on the collective modes for − 350 mT, − 200 mT and 0 mT as shown in Fig. 3, and the corresponding ground states are the $p = 1$ target skyrmion at high field, the $p = -1$ target skyrmion with 2π central skyrmion and the $p = -1$ target skyrmion at zero field, respectively.

The collective modes at zero field are analyzed first. As discussed above, twelve significant modes (defined as A1–A12) can be identified in the spectrum at zero field. Mode A1 (Fig. 4a), at 1.45 GHz, has two nodes in the radial direction. There are four nodes in the azimuthal direction spaced equally along the circumference. There is one node in the vertical direction (Fig. 5a) along the outer circumference, but it does not bisect the core. Mode A2 (Fig. 4b) at 2.70 GHz is similar to

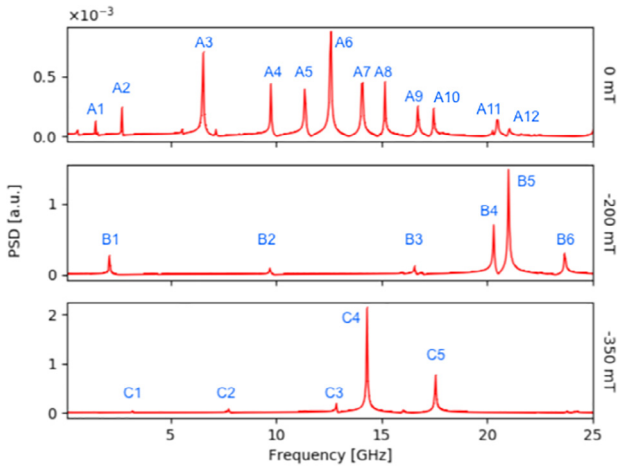


Fig. 3. PSDs for 0 mT (top), − 200 mT (middle) and − 350 mT (bottom), respectively.

mode A1 with one radial node located in the center, but it has zero azimuthal nodes. Like mode A1, there is also one node in the vertical direction (Fig. 5b), but in this case it extends through the core. Similar to modes A1 and A2, mode A3 at 6.55 GHz (Fig. 4c) has two radial nodes, one close to the center and one close to the edge. A3 also has four azimuthal nodes spaced equally around the outer edge similar to mode A1. In contrast to modes A1 and A2, mode A3 has two vertical nodes that bisect the core (Fig. 5c). Mode A4 (Fig. 4d) at 9.75 GHz has two nodes in the radial direction. It has eight nodes in the azimuthal direction that are equally spaced around the outer edge, but the size of these nodes are not evenly distributed along the circumference. There are also four weak nodes near the center of the disk. The vertical nodes of mode A4 (Fig. 5d) are more subtle; there are two nodes that bisect the core, but do not extend to the outer edge. Mode A5 in Fig. 4e, at 11.35 GHz, has three radial nodes. It has three types of nodes in the azimuthal direction spaced equally on three different concentric rings rather than the same ring and each of them has four nodes. Mode A5 has one vertical node that bisects the outer edge ring and two vertical nodes that bisect the core (Fig. 5e). Mode A6 (Fig. 4f), at 12.60 GHz has two radial nodes. It has eight crescent shaped elongated nodes at the edge and four weak nodes near the center in the azimuthal direction. In the vertical direction, there is one node that bisects the outer ring, but does not penetrate the core and there are two vertical nodes near the core (Fig. 5f).

Mode A7 shown in Fig. 6a at 14.07 GHz, has two radial nodes and eight nodes in the azimuthal direction spaced equally along the other edge. It has three vertical nodes that bisect the outer edge (Fig. 7a). Mode A8 at 15.15 GHz, as seen in Fig. 6b, like all prior modes resolved at 0 mT, has two radial nodes. Similar to modes A1 and A3, there are four nodes in the azimuthal direction spaced equally along the outer edge. There are also four very weak azimuthal nodes near the center of the disk. In the vertical direction, mode A8 has two nodes that cut through the entire disk (Fig. 7b). Mode A9, at 16.70 GHz has three radial nodes (Fig. 6c). There are twelve azimuthal nodes spaced equally around the outer edge, but their amplitudes are relatively small. There are also four azimuthal nodes distributed equally near the center and four connected azimuthal nodes at the inner core. In the vertical direction, mode A9 has three nodes that bisect the core only (Fig. 7c). Mode A10 (Fig. 6d), at 17.45 GHz, has two radial nodes and four elongated azimuthal nodes near the outside edge. There are also four weak nodes in the azimuthal direction near the center. In the vertical direction, mode A10 has two nodes bisecting both the outer edge and core (Fig. 7d). Mode A11 (Fig. 6e), at 20.48 GHz, has two radial nodes and eight elongated azimuthal nodes at the disk edge. It has two vertical nodes that bisect the outer edge (Fig. 7e). The radial azimuthal modse of Mode A12 (Fig. 6f) at 21.05 GHz are complicated. It has two radial nodes, one close to the center has very small amplitude and another one close to the edge. There are twelve azimuthal nodes with three different shapes at the disk edge. In the vertical direction, mode A12 has one node near the core and two nodes that bisect the edge (Fig. 7f).

Among all these modes at zero field, only modes A5 and A9 have three radial nodes and A2 is the only mode without any azimuthal nodes. Comparing the in-plane spatial map of the collective modes at zero magnetic field, it is obvious that mode A1, A2, A3 and A9 have relatively strong response at the core, while the rest of the modes have relatively strong response at the edge. These results are also consistent with the out-of-plane spatial maps, where similar behavior can be spotted. The collective modes discussed above successfully reflect the spin texture of a target skyrmion, where the modes near the center are originated from the central skyrmion and the modes at the edge are originated from the outer helical ring.

Next, we look at the modes resolved at − 200 mT, where the ground state is a $p = -1$ target skyrmion with a 2π central skyrmion. There are six significant modes in the spectrum, defined as B1-B6. Mode B1 at 2.1 GHz has three nodes in the radial direction and no azimuthal node (Fig. 8a). Its vertical mode is uniform and thus has no vertical node

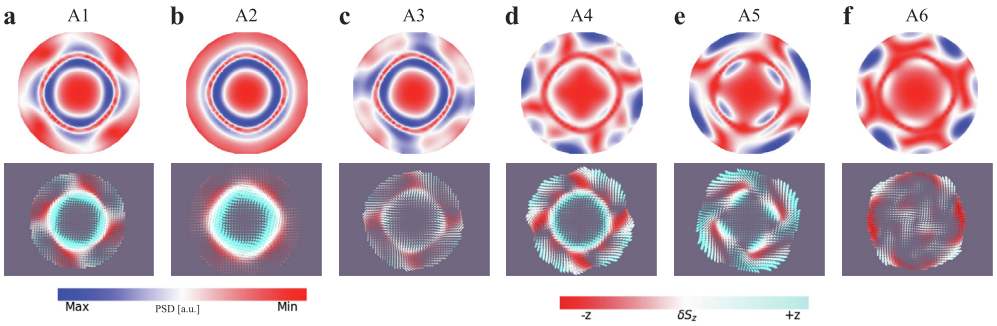


Fig. 4. Spatial Fourier transformation (top) and snapshot of the real time dynamics (bottom) of $\delta S_z(t)$ resolved at 0 mT. Top surfaces of the disk for modes A1–A6 are shown.

(Fig. 9a). Mode B2 at 9.7 GHz has three nodes in the radial direction and no azimuthal nodes (Fig. 8b). There are two vertical nodes that bisect the disk (Fig. 9b). Mode B3 at 16.55 GHz only has two radial nodes located in the center and in a surrounding inner ring. It has four nodes in the azimuthal direction located near the center and along the outer edge (Fig. 8c). It has one vertical node in the center that bisects the entire spin texture and three vertical nodes located between the edge and the center (Fig. 9c). Mode B4 at 20.31 GHz has three nodes in the radial direction located in the center and an inner and outer concentric ring (Fig. 8d). There are no azimuthal nodes. There are three vertical nodes that penetrate the core in the center and near the top and bottom faces of the disk (Fig. 9d). Mode B5 at 21 GHz (Fig. 8e) has three nodes in the radial direction. It has eight azimuthal nodes at the edge and four azimuthal nodes near the center. B5 has one vertical node in the outer concentric ring that does not penetrate the core and two vertical nodes near the center (Fig. 9e). Finally, mode B6 at 23.66 GHz, has three nodes in the radial direction (Fig. 8f). It also has eight azimuthal nodes at the edge and four azimuthal nodes near the center, which is almost the same with mode B5. But the vertical nodes of B6 are very different from B5. B6 has two vertical nodes that pierce the outer rings, but do not penetrate the core and there is one vertical node that penetrates the core halfway along the disk (Fig. 9f).

All the collective modes at − 200 mT have three radial modes except mode B3, which only has two radial modes and a strong azimuthal mode. B1 is the only mode that hosts a uniform vertical mode. Modes B1, B2 and B4 have strong oscillation amplitude at the center of the disk, while the oscillation amplitude of B6 at the edge and at the center are both very strong. The in-plane spatial maps of B5 and B6 are very similar with each other and they all have strong responses at the edge, but their out-of-plane spatial maps are quite different. Comparing with modes A1–A12, modes B1–B6 directly reflects the spin textures of the target skyrmion with a 2π central skyrmion.

Finally, we analyze the five significant modes at − 350 mT, hereafter referred to as modes C1–C5. Mode C1 at 3.2 GHz, show in Fig. 10a has two nodes in the radial direction. There are no nodes in the azimuthal direction. In the vertical direction, there is one node located halfway along the depth of the disk that bisects the outside and inner core (Fig. 11a). Mode C2 at 7.75 GHz has two nodes in the radial direction and no nodes in the azimuthal direction (Fig. 10b). It has two nodes in the vertical direction (Fig. 11b). In mode C3 (12.85 GHz), shown in (Fig. 10c), there are two nodes in the radial direction. One is near the center and the other one is localized in a concentric ring at the edge. There are no nodes in the azimuthal direction and no nodes in the vertical direction (Fig. 11c). The radial symmetry of the nodes reflect the underlying symmetry of the ground state target skyrmion under large magnetic field. Similar to mode C3, mode C4 (14.3 GHz) shown in Fig. 10d also has two nodes in the radial direction located in the center and a surrounding ring. It has no azimuthal node, but there is a tendency to form eight azimuthal nodes at the edge and four azimuthal nodes at the center. In contrast to mode C3, mode C4 has one node in the vertical direction located halfway along the depth of the disk that cuts through the outer ring of magnetization fluctuations and most of the way through the inner core (Fig. 11d). Mode C5 at 17.55 GHz, shown in Fig. 10e is similar to modes C3 and C4 in that it is also has two nodes in the radial direction, located at the center and in a concentric ring and no nodes in the azimuthal direction. It has the tendency to form four azimuthal nodes at the center. In contrast to both modes C3 and C4, mode C5 has two nodes in the vertical direction located approximately 1/3 and 2/3 the length of the disk, both bisecting the outer ring and inner core (Fig. 11e).

From the collective modes at − 350 mT, it is obvious that under strong magnetic fields (along z direction) it is difficult for the target skyrmion to develop any low-energy azimuthal modes. But the radial modes and vertical modes can still survive since they have close relation with the ferromagnetic resonance modes in this geometry. Modes C3–C5 have both strong response at the center and at the edge, while the responses of C1 and C2 are only strong at the center. Furthermore, the in-plane spatial maps of these collective modes show the features of the hybridized breathing mode, which is similar to that of a 2D skyrmion [29]. Animations of all the resonance modes discussed above are shown in the Supplemental materials.

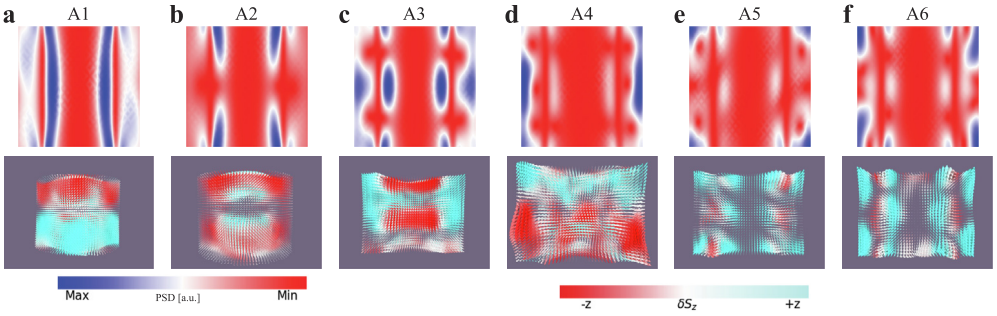


Fig. 5. Spatial Fourier transformation (top) and snapshot of the real time dynamics (bottom) of $\delta S_z(t)$ resolved at 0 mT. $x-z$ plane views of modes A1–A6 are shown.

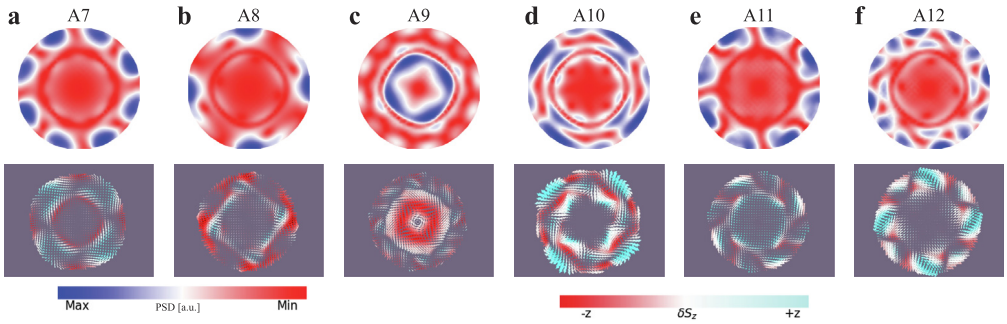


Fig. 6. Spatial Fourier transformation (top) and snapshot of the real time dynamics (bottom) of $\delta S_z(t)$ resolved at 0 mT. Top surfaces of the disk for modes A7–A12 are shown.

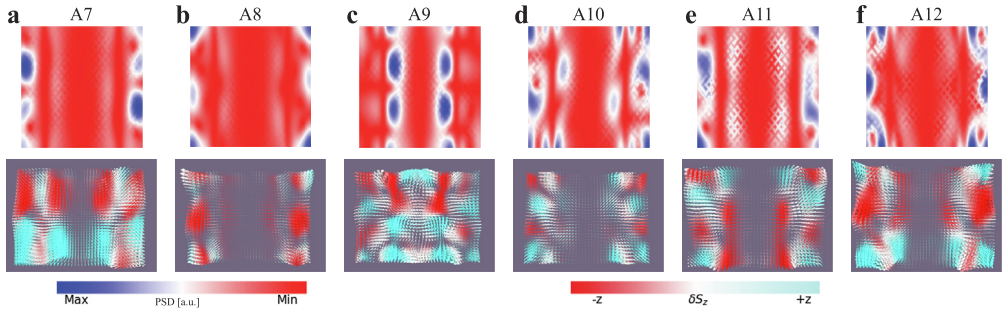


Fig. 7. Spatial Fourier transformation (top) and snapshot of the real time dynamics (bottom) of $\delta S_z(t)$ resolved at 0 mT. $x-z$ plane views of modes A7–A12 are shown.

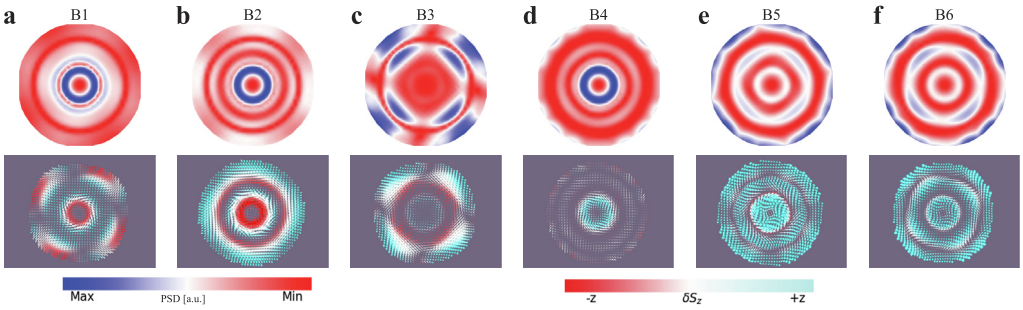


Fig. 8. Spatial Fourier transformation (top) and snapshot of the real time dynamics (bottom) of $\delta S_z(t)$ resolved at − 200 mT. Top surfaces of the disk for modes B1–B6 are shown.

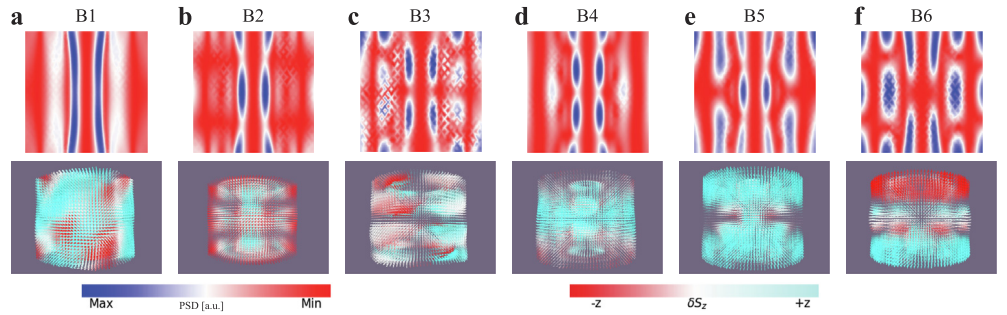


Fig. 9. Spatial Fourier transformation (top) and snapshot of the real time dynamics (bottom) of $\delta S_z(t)$ resolved at − 200 mT. $x-z$ plane views of modes B1–B6 are shown.

5. Discussions and conclusions

After analyzing all the collective modes above, we can clearly see the differences between the collective modes in 2D and 3D. Due to the presence of finite thickness, resonant modes along the disk axis direction are developed, which could enrich the possible modes hosted by the skyrmion. For very thin disk, uniform collective modes along the disk normal direction are more energy favorable, it is difficult to excite vertical collective modes in this case. When the disk thickness is comparable with or even larger than the helical period, it is much easier to develop these collective modes along the disk normal direction due to the nature of spin waves and helimagnets. So the thickness of the disk has to be comparable to the helical period L_D of the material in order to get visible effect of the collective modes along the disk normal

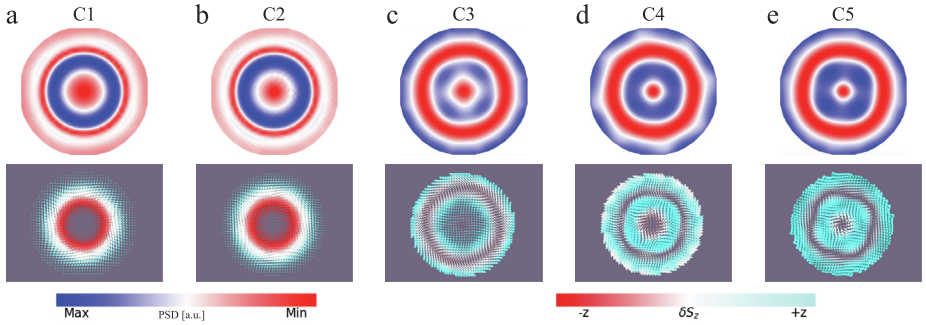


Fig. 10. Spatial Fourier transformation (top) and snapshot of the real time dynamics (bottom) of $\delta S_z(t)$ resolved at − 350 mT. Top surfaces of the disk for modes C1–C5 are shown.

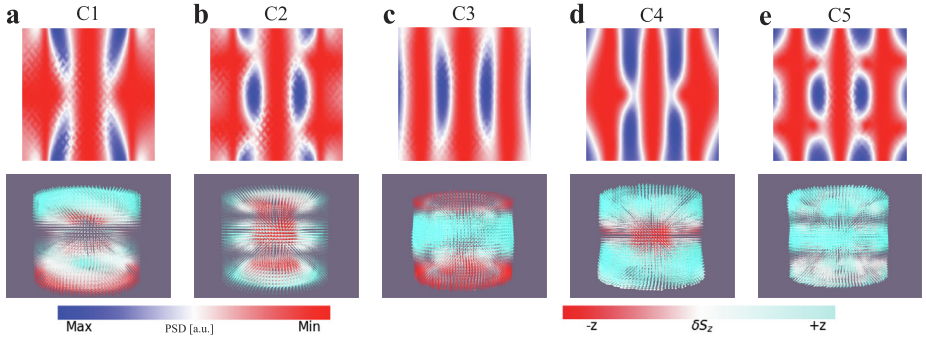


Fig. 11. Spatial Fourier transformation (top) and snapshot of the real time dynamics (bottom) of $\delta S_z(t)$ resolved at − 350 mT. $x - z$ plane views of modes C1–C5 are shown.

direction. Compared to the skyrmion resonant modes in 2D, there are strong hybridizations of different 2D simple modes in 3D. For example, the pure breathing mode is missing in the collective modes discussed above. It is hybridized with other modes, such as the radial and azimuthal spin wave modes and even vertical spin wave modes. Thus, to study these hybridized modes, it is also important to understand the simple modes first from simple geometries like 2D nanodisk and one dimensional nanowire [32]. We also notice that in the vicinity of the discontinuities in the spectrum, the dynamical response of skyrmion is really strong (not shown here). This suggests that it is possible to switch the polarity of skyrmion using the corresponding collective modes, which might be an energy efficient way to manipulate target skyrmions [33,34].

Detailed analysis of the collective modes also suggest that 2D spatial map alone is *not* enough to distinguish all the different modes. The out-of-plane spatial maps are also necessary in order to get a complete understanding of the resonant modes. Collectively, this provides strong evidence that the resonant modes of 3D spin textures require investigations in multiple planes in order to be characterized. This might be challenging experimentally, but the recent discovered 3D X-ray vector tomography [30] and the related techniques [31] may shed light on the 3D mapping of resonant modes.

The current simulations were performed at zero temperature and in a perfect sample. In real experiments, the presence of disorders (e.g., edge or point defects) and finite temperature may potentially modify the calculated spectrum and patterns of the collective modes. For disorders, as suggested by previous studies[18–20], they can affect the skyrmion dynamics in many ways, e.g., reducing the threshold of depinning force, changing the trajectory of skyrmion motion, etc. For isolated, geometrically confined systems such as the target skyrmion under discussion here, we may expect the role of disorder in several aspects. For weak disorder, the modes with small PSD amplitudes might be washed out if the target skyrmion's responses to the a.c. magnetic fields are not enough to overcome the pinning force. Those modes with strong amplitudes can still persist due to their strong responses. In this sense, the driving force (amplitude of the a.c. magnetic field here) becomes important for the resonant modes, which is quite different from the disorder free case. Furthermore, the spatial patterns of different modes can vary from their original spatial patterns depending on the distribution or the type of defects. For strong disorder, even the ground state spin texture of the target skyrmion may change, so the spectrum may change according to the spin textures.

For finite temperature, broadening of the resonance peak is expected. The spectrum would not be fundamentally different, although there might be some modulations of the individual modes. Furthermore, spatial patterns of the resonant mode should still preserve their features at finite temperature. Therefore, even in the presence of moderate finite temperature and disorders, the collective modes and their spatial features are still measurable.

In conclusion, the response of a target skyrmion to a.c. magnetic field is investigated using micromagnetic simulations. The full power spectrum is calculated and it shows that the finite thickness of the target skyrmion can result in complex behaviors of the resulting resonant modes. Dynamical simulations are employed to resolve individual resonant modes at the ground state of a $p = 1$ target skyrmion at high field, a $p = -1$ target skyrmion with 2π central skyrmion and a $p = -1$ target skyrmion at zero field, respectively. It is shown that the target skyrmion hosts 3D collective modes due to its 3D nature. There are cases in which the in-plane behavior alone is not enough to fully characterize a mode and the out-of-plane becomes important, also reflecting the three-dimensional nature of the spin texture. The collective modes studied here could be experimentally excited by applying a.c. magnetic fields via coplanar waveguides or microcoils with specific shapes [35]. Successful characterization of the resonant modes is crucial to the prospect of using the target skyrmion as a basic unit in future spintronic devices. Methodology developed in this work provides a blueprint for studying resonant modes of any other 3D magnetic structures.

Acknowledgements

We acknowledge fruitful discussions with Hang Li. This work was supported by the U.S. Department of Energy (DOE), Office of Science, Basic Energy Sciences (BES) under Award No. de-sc0016424. Y.L. acknowledges supports from the National Natural Science Foundation of China (NSFC Grant No. 11804380) and the Institute of Physics, Chinese Academy of Sciences through the International Young Scientist Fellowship (Grant No. 2018001).

Appendix A. Supplementary data

Supplementary data associated with this article can be found, in the online version, athttps://doi.org/10.1016/j.jmmm.2019.165447.

References

[1] A. Fernández-Pacheco, R. Streubel, O. Fruchart, R. Hertel, P. Fischer, R.P. Cowburn, Three-dimensional nanomagnetism, Nat. Commun. 8 (2017) 15756, https://doi.org/10.1038/ncomms15756.
[2] A. Fert, N. Reyren, V. Cros, Magnetic skyrmions: advances in physics and potential applications, Nat. Rev. Mater. 2 (7) (2017) 17031, https://doi.org/10.1038/natrevmats.2017.31.
[3] S.S.P. Parkin, M. Hayashi, L. Thomas, Magnetic domain-wall racetrack memory, Science 320 (5873) (2008) 190–194, https://doi.org/10.1126/science.1145799.
[4] N. Nagaosa, Y. Tokura, Topological properties and dynamics of magnetic skyrmions, Nat. Nanotechnol. 8 (12) (2013) 899–911, https://doi.org/10.1038/nnano.2013.243.
[5] F.N. Rybakov, A.B. Borisov, S. Blügel, N.S. Kiselev, New type of stable particlelike states in chiral magnets, Phys. Rev. Lett. 115 (11) (2015) 117201, , https://doi.org/10.1103/PhysRevLett. 115.117201.
[6] P. Sutcliffe, Skyrmion knots in frustrated magnets, Phys. Rev. Lett. 118 (24) (2017) 247203, , https://doi.org/10.1103/PhysRevLett. 118.247203.
[7] Y. Liu, R.K. Lake, J. Zang, Binding a hopfion in a chiral magnet nanodisk, Phys. Rev. B 98 (17) (2018) 174437, https://doi.org/10.1103/PhysRevB.98.174437.
[8] F. Zheng, F.N. Rybakov, A.B. Borisov, D. Song, S. Wang, Z.-A. Li, H. Du, N.S. Kiselev, J. Caron, A. Kovács, M. Tian, Y. Zhang, S. Blügel, R.E. Dunin-Borkowski, Experimental observation of chiral magnetic bobbers in B20-type FeGe, Nat. Nanotechnol. 13 (6) (2018) 451, https://doi.org/10.1038/s41565-018-0093-3.
[9] M. Redies, F.R. Lux, J.-P. Hanke, P.M. Buhl, G.P. Müller, N.S. Kiselev, S. Blügel, Y. Mokrousov, Distinct magnetotransport and orbital fingerprints of chiral bobbers. arXiv:1811.01584 [cond-mat].
[10] I. Dzyaloshinsky, A thermodynamic theory of "weak" ferromagnetism of antiferromagnetics, J. Phys. Chem. Solids 4 (4) (1958) 241–255, https://doi.org/10.1016/0022-3697(58)90076-3.
[11] T. Moriya, Anisotropic superexchange interaction and weak ferromagnetism, Phys. Rev. 120 (1) (1960) 91–98, https://doi.org/10.1103/PhysRev. 120.91.
[12] H.S. Park, X. Yu, S. Aizawa, T. Tanigaki, T. Akashi, Y. Takahashi, T. Matsuda, N. Kanazawa, Y. Onose, D. Shindo, A. Tonomura, Y. Tokura, Observation of the magnetic flux and three-dimensional structure of skyrmion lattices by electron holography, Nat. Nanotechnol. 9 (5) (2014) 337–342, https://doi.org/10.1038/nnano.2014.52.
[13] M. Beg, R. Carey, W. Wang, D. Cortés-Ortuño, M. Vousden, M.-A. Bisotti, M. Albert, D. Chernyshenko, O. Hovorka, R.L. Stamps, H. Fangohr, Ground state search, hysteretic behaviour, and reversal mechanism of skyrmionic textures in confined helimagnetic nanostructures, Scientific Rep. 5 (2015) 17137, https://doi.org/10.1038/srep17137.
[14] H. Du, R. Che, L. Kong, X. Zhao, C. Jin, C. Wang, J. Yang, W. Ning, R. Li, C. Jin, X. Chen, J. Zang, Y. Zhang, M. Tian, Edge-mediated skyrmion chain and its collective dynamics in a confined geometry, Nat. Commun. 6 (2015) 8504, https://doi.org/10.1038/ncomms9504.
[15] C. Jin, Z.-A. Li, A. Kovács, J. Caron, F. Zheng, F.N. Rybakov, N.S. Kiselev, H. Du, S. Blügel, M. Tian, Y. Zhang, M. Farle, R.E. Dunin-Borkowski, Control of morphology and formation of highly geometrically confined magnetic skyrmions, Nat. Commun. 8 (2017) 15569, https://doi.org/10.1038/ncomms15569.
[16] B. Das, B. Balasubramanian, R. Skomski, P. Mukherjee, S.R. Valloppilly, G.C. Hadjipanayis, D.J. Sellmyer, Effect of size confinement on skyrmionic properties of MnSi nanomagnets, Nanoscale 10 (20) (2018) 9504–9508, https://doi.org/10.1039/C7NR08864G.
[17] H. Du, W. Ning, M. Tian, Y. Zhang, Magnetic vortex with skyrmionic core in a thin nanodisk of chiral magnets, Europhys. Lett. 101 (3) (2013) 37001, https://doi.org/10.1209/0295-5075/101/37001.
[18] Shintaro Hoshino, Naoto Nagaosa, Theory of the magnetic skyrmion glass, Phys. Rev. B 97 (2) (January 2018) 024413, , https://doi.org/10.1103/PhysRevB.97.024413.
[19] C. Reichhardt, C.J. Olson Reichhardt, Depinning and nonequilibrium dynamic phases of particle assemblies driven over random and ordered substrates: a review, Rep. Prog. Phys. 80 (2) (2016) 026501, , https://doi.org/10.1088/1361-6633/80/2/026501.
[20] C. Reichhardt, D. Ray, C.J. Olson Reichhardt, Collective transport properties of driven skyrmions with random disorder, Phys. Rev. Lett. 114 (21) (2015) 217202, , https://doi.org/10.1103/PhysRevLett. 114.217202.
[21] A.O. Leonov, U.K. Rößler, M. Mostovoy, Target-skyrmions and skyrmion clusters in nanowires of chiral magnets, EPJ Web Conf. 75 (2014) 05002, , https://doi.org/10.1051/epjconf/20147505002.
[22] F. Zheng, H. Li, S. Wang, D. Song, C. Jin, W. Wei, A. Kovács, J. Zang, M. Tian, Y. Zhang, H. Du, R.E. Dunin-Borkowski, Direct imaging of a zero-field target skyrmion and its polarity switch in a chiral magnetic nanodisk, Phys. Rev. Lett. 119 (19) (2017) 197205, , https://doi.org/10.1103/PhysRevLett. 119.197205.
[23] A. Bogdanov, A. Hubert, The stability of vortex-like structures in uniaxial ferromagnets, J. Magn. Magn. Mater. 195 (1) (1999) 182–192, https://doi.org/10.1016/S0304-8853(98)01038-5.
[24] M. Beg, M. Albert, M.-A. Bisotti, D. Cortés-Ortuño, W. Wang, R. Carey, M. Vousden, O. Hovorka, C. Ciccarelli, C.S. Spencer, C.H. Marrows, H. Fangohr, Dynamics of skyrmionic states in confined helimagnetic nanostructures, Phys. Rev. B 95 (1) (2017) 014433, , https://doi.org/10.1103/PhysRevB.95.014433.
[25] Y. Liu, R.K. Lake, J. Zang, Shape dependent resonant modes of skyrmions in magnetic nanodisks, J. Magn. Magn. Mater. 455 (2018) 9–13, https://doi.org/10.1016/j.jmmm.2017.07.007.
[26] A. Vansteenkiste, J. Leliaert, M. Dvornik, M. Helsen, F. Garcia-Sanchez, B. Van Waeyenberge, The design and verification of MuMax3, AIP Adv. 4 (10) (2014) 107133, , https://doi.org/10.1063/1.4899186.
[27] L. Landau, E. Lifshitz, On the theory of the dispersion of magnetic permeability in ferromagnetic bodies, Phys. Z. Sowjetunion 8 (153) (1935) 101–114.
[28] T.L. Gilbert, A phenomenological theory of damping in ferromagnetic materials, IEEE Trans. Magn. 40 (6) (2004) 3443–3449, https://doi.org/10.1109/TMAG.2004.836740.
[29] J.-V. Kim, F. Garcia-Sanchez, J. Sampaio, C. Moreau-Luchaire, V. Cros, A. Fert, Breathing modes of confined skyrmions in ultrathin magnetic dots, Phys. Rev. B 90 (6) (2014) 064410, , https://doi.org/10.1103/PhysRevB.90.064410.
[30] C. Donnelly, M. Guizar-Sicairos, V. Scagnoli, S. Gliga, M. Holler, J. Raabe, L.J. Heyderman, Three-dimensional magnetization structures revealed with X-ray vector nanotomography, Nature 547 (7663) (2017) 328–331, https://doi.org/10.1038/nature23006.
[31] P. Fischer, J. Phys. D: Appl. Phys. 50 (31) (2017) 313002, , https://doi.org/10.1088/1361-6463/aa778a.
[32] R. Skomski, M. Chipara, D.J. Sellmyer, Spin-wave modes in magnetic nanowires, J. Appl. Phys. 93 (10) (2003) 7604–7606, https://doi.org/10.1063/1.1558691.
[33] B. Zhang, W. Wang, M. Beg, H. Fangohr, W. Kuch, Microwave-induced dynamic switching of magnetic skyrmion cores in nanodots, Appl. Phys. Lett. 106 (10) (2015) 102401, , https://doi.org/10.1063/1.4914496.
[34] Y. Liu, H. Du, M. Jia, A. Du, Switching of a target skyrmion by a spin-polarized current, Phys. Rev. B 91 (9) (2015) 094425, , https://doi.org/10.1103/PhysRevB.91.094425.
[35] F. Büttner, C. Moutafis, M. Schneider, B. Krüger, C.M. Günther, J. Geilhufe, C.v.K. Schmising, J. Mohanty, B. Pfau, S. Schaffert, A. Bisig, M. Foerster, T. Schulz, C.a.F. Vaz, J.H. Franken, H.J.M. Swagten, M. Kläui, S. Eisebitt, Dynamics and inertia of skyrmionic spin structures, Nat. Phys. 11 (3) (2015) 225–228, https://doi.org/10.1038/nphys3234.